Colloids and Surfaces B: Biointerfaces 68 (2009) 61–67

Contents lists available at ScienceDirect

Colloids and Surfaces B: Biointerfaces

journal homepage: www.elsevier.com/locate/colsurfb

# Hysteresis behavior of amphiphilic model peptide in lung lipid monolayers at the air–water interface by an IRRAS measurement

Hiromichi Nakahara[a], Anna Dudek[b], Yoshihiro Nakamura[c], Sannamu Lee[d], Chien-Hsiang Chang[b], Osamu Shibata[a,*]

[a] Department of Biophysical Chemistry, Faculty of Pharmaceutical Sciences, Nagasaki International University, 2825-7 Huis Ten Bosch, Sasebo, Nagasaki 859-3298, Japan
[b] Department of Chemical Engineering, National Cheng Kung University, Tainan 70101, Taiwan, ROC
[c] Muromachi Chemical Co. Ltd., Ohmuta, Fukuoka 836-0895, Japan
[d] Department of Chemistry, Faculty of Science, Fukuoka University, Fukuoka 814-0180, Japan

ARTICLE INFO

*Article history:*
Received 24 July 2008
Received in revised form
12 September 2008
Accepted 14 September 2008
Available online 21 September 2008

*Keywords:*
Pulmonary surfactant
Respiratory distress syndrome
Langmuir monolayer
DPPC
IRRAS

ABSTRACT

Pulmonary functions such as rapid adsorption, respreading, and hysteresis behavior of pulmonary surfactants are very important for respiratory movement. The interfacial behavior of pulmonary preparations containing an amphiphilic peptide (Hel 13-5) has recently investigated. An orientation of hydrophobic chains in a dipalmitoylphosphatidylcholine (DPPC) with or without palmitic acid (PA) is associated with a collapse of alveoli during respiration process. Therefore, the present study focused on the acyl chain orientation in model pulmonary surfactants (DPPC/Hel 13-5 and DPPC/PA/Hel 13-5). A successive change in the orientation during cyclic compression and expansion of films at the air–water interface can be probed directly by an infrared reflection–absorption spectrometry (IRRAS) technique. The hysteresis behavior, one of very important pulmonary functions, was previously observed in surface pressure ($\pi$)–molecular area ($A$) isotherms for the both model pulmonary surfactant systems (*Langmuir* 22(2006)1182-1192 and *Langmuir* 22(2006)5792-5803). In addition, it was reported that Hel 13-5 was squeezed-out of the surface on compression like native pulmonary surfactant proteins. The data obtained for the binary and ternary systems were compared with those of the equivalent pure DPPC and DPPC/PA mixtures, respectively. For an asymmetric methylene stretching vibration ($\nu_a$-$CH_2$) RA intensity, the absolute RA values increased with shifting to small surface area, monotonously. For the corresponding wavenumber, on the other hand, the values gradually decreased into ~2920 $cm^{-1}$. However, they were kept constant in the squeeze-out region in spite of a further decrease of surface area. These results suggested that the orientation of hydrophobic chains in DPPC and DPPC/PA mixtures became in the most packed state soon after emergence of the squeeze-out process of Hel 13-5 and then the packed orientation was retained up to the collapse state. This indicated that the squeezed-out Hel 13-5 stabilized monolayers left at the interface. For the DPPC/PA/Hel 13-5 system, in particular, dissociated PA molecules were excluded together with Hel 13-5 and the surface monolayers were refined to DPPC and undissociated PA components during the compression process. And the similar behavior in the second and third cycles supported the good respreading ability of the monolayers containing Hel 13-5.



## 1. Introduction

A pulmonary surfactant is a complex mixture of multiple lipids (~90 wt.%) and four surfactant proteins (SP-A, -B, -C, and -D, ~10 wt.%) [1–3]. It aids significant functions in the alveoli such as the defense from exotic viruses and bacteria, and the prevention of alveolar collapse during respiration. The main lipid component of the surfactant is dipalmitoylphosphatidylcholine (DPPC) and it can retain high surface pressure (or low surface tension) in monolayer and multilayer states at the air–water interface on film compression. However, the spreading rate of ordered DPPC to the interface under film expansion process is too slow and it is a main defect of DPPC molecules for pulmonary functions [4]. Two relatively small hydrophobic surfactant proteins, SP-B and SP-C, promote the spreading and adsorption of DPPC from close-packed states and vesicular aggregates. The molecular basis remains obscure,

* Corresponding author. Tel.: +81 956 20 5686; fax: +81 956 20 5686.
*E-mail addresses:* wosamu@niu.ac.jp, wosamu-s@hotmail.co.jp (O. Shibata).
*URL:* http://www.niu.ac.jp/ pharm1/lab/physchem/indexenglish.html (O. Shibata).

0927-7765/$ – see front matter © 2008 Elsevier B.V. All rights reserved.
doi:10.1016/j.colsurfb.2008.09.013

although there are many experimental evidences for these actions [5,6]. This is thought to be due to large molecular structures of SP-B and SP-C compared with lipids in pulmonary surfactants. Therefore, SP-B and SP-C analogous peptides such as KL4, rSP-C, and Hel 13-5 have been utilized to clarify the pulmonary functions [7–9]. Palmitic acid (PA) is present in a relatively lower amount in pulmonary extracts compared with DPPC, but it is a very important additive for the proper functioning of both natural and synthetic pulmonary surfactants. The aliphatic chains of DPPC monolayers are declined to the normal even in the most packed state due to their large head groups [10–13]. However, it has been mentioned that a small amount of PA to DPPC monolayers improves their acyl chain orientation [13–15]. Furthermore, the addition of ~10 wt.% PA to pulmonary surfactants extracted from animals has induced a significant improvement in their properties both *in vitro* and *in vivo* [16,17].

To investigate the *in situ* behavior at the air–alveolar interface during respiration process is extremely difficult. Thus, monolayers at the air–water interface have been intensely adopted as experimental paradigms for elucidating the interfacial properties and mechanisms of pulmonary surfactants [7–9]. The morphological phase behavior of monolayers at the air–water interface under compression and expansion could be observed by optical techniques such as Brewster angle microscopy (BAM) [18–20], fluorescence microscopy (FM) [21–23], and atomic force microscopy (AFM) [24–26]. In addition, the conformational and orientational information about film components could be understood using a spectroscopic method such as an infrared reflection–absorption spectrometry (IRRAS) [27–29]. Recently, very interesting studies on biosensor for $Ca^{2+}$ and organophosphorus compounds have been reported from the view point of Langmuir monolayer utilizing IRRAS and polarization-modulated IRRAS [30,31]. The variation in the orientation and structure of the specific host protein monolayers was probed and analyzed before and after binding the corresponding guest molecules in detail.

So far, the authors have targeted an arc light on newly designing pulmonary surfactant preparations and elucidating the interfacial biophysical behavior and mechanism of SP-B during respiration using the model peptide (Hel 13-5), which is a 18-mer amphiphilic peptide and exerts effective pulmonary functions in lipid mixtures [9,24,32,33]. The interfacial behavior of spread monolayers for many kinds of synthetic pulmonary surfactants has been systematically investigated employing Langmuir [surface pressure ($\pi$)–area ($A$) and surface potential ($\Delta V$)–$A$] isotherms, FM images, and AFM images. For example, Hel 13-5 peptides facilitate and improve surface adsorption of DPPC molecules from vesicular aqueous solutions [24]. However, the behavior has not been considered from the view point of spectroscopic aspects, yet.

In the current study, the authors have applied the *in situ* IRRAS technique to investigate a variation in acyl chain conformation and orientation of DPPC and DPPC/PA monolayers against the Hel 13-5 addition during repeated compression and expansion. The hysteresis $\pi$–$A$ isotherms in the pulmonary surfactant systems have been reported before [24,32,34–36]. Therefore, the binary system (DPPC/Hel 13-5) and the ternary system (DPPC/PA/Hel 13-5) were used here to acquire further understanding of the relationship between spectroscopic and thermodynamic data. Moreover, the data obtained for the binary and ternary systems were compared with those of the equivalent pure DPPC and DPPC/PA mixtures to carry out a quantitative comparison, respectively. The present work will provide a further understanding of the facilitation of respreading by the Hel 13-5 addition and of the mechanism for surface refining by the squeeze-out behavior.

## 2. Materials and methods

### 2.1. Materials

Hel 13-5 (MW: 2203 Da) was synthesized by Fmoc strategy based on the solid phase technique starting from Fmoc-Leu-PEG-PS resin (0.1 m mol scale) with Perseptive 9050 automatic peptide synthesizer and purified by HPLC with reversed-phase column (20 mm × 250 mm, YMC C8) as described previously [37]. Dipalmitoylphosphatidylcholine (DPPC, purity >99%) and palmitic acid (PA, purity >99%) were obtained from Avanti Polar Lipids, Inc (Alabaster, AL, USA) and Sigma (St. Louis, MO, USA), respectively. It was used without further purification or characterization. *n*-Hexane (>99%) was came from Tedia Company Inc. (Fairfield, OH, USA) and ethanol (~99.5%) was purchased from Seoul Chemical Industry Co., Ltd. (Korea). The *n*-hexane/ethanol (=9:1, 9:1, and 4.5:5.5, v/v) mixtures were used as the spreading solvents for DPPC, PA, and Hel 13-5, respectively. The water used in all experiments was purified by means of a Milli-Q plus water purification system (Millipore) with a resistivity of 18.2 MΩ cm and surface tension of 72.7 mN $m^{-1}$ at 293.2 K. A buffer solution of $NaH_2PO_4/Na_2HPO_4$ with a pH value of 7.0 was used to prepare the aqueous subphase.

### 2.2. Methods

An infrared reflection–absorption spectrometry analysis was conducted using a PerkinElmer FTIR spectrometer (model Spectrum GX) with a liquid-nitrogen-cooled mercury cadmium telluride (MCT) detector [29]. A monolayer/grazing angle accessory (P/N 19650 series, Specac Inc.) with a removable Teflon Langmuir trough was used with the FTIR spectrometer to obtain the IR spectrum of a monolayer at the air/liquid interface. Measurements were performed at room temperature (~303.2 K). The IR spectra were taken using unpolarized light with an angle of incidence of 40°, as measured perpendicular to the liquid surface. The sample chamber of the FTIR spectrometer was continuously purged with dry air from a purge gas generator. Spectra were collected at 8 $cm^{-1}$ resolution with a scan number of 128. All of the spectra were reported by subtracting the buffer spectrum from the measured spectra. When the IRRAS analysis of a monolayer at a continuously compressed-expanded air/liquid interface was conducted, the removable Langmuir trough of the monolayer/grazing angle accessory was filled with 8 mL of buffer solution with a pH value of 7.0. The 3.4 μL DPPC (1.0 mM), 7.1 μL DPPC/Hel 13-5 at $X_{Hel\ 13\text{-}5}$ = 0.1 (0.53 mM), 4.5 μL DPPC/PA (1.0 mM), or 9.4 μL DPPC/PA/Hel 13-5 solutions at $X_{Hel\ 13\text{-}5}$ = 0.1 (0.53 mM) were spread at the interface by using a 10 μL microsyringe (Hamilton Co.). These spreading volumes were selected to quantitatively compare with the appropriate $\nu_a$-$CH_2$ IR peaks. That is, $2.0 \times 10^{15}$ DPPC or $2.7 \times 10^{15}$ DPPC/PA molecules were spread to the interface in the binary or ternary systems, respectively. After a period of 20 min was allowed for solvent evaporation, the spread monolayer was continuously compressed and then expanded by a barrier at a rate of 1 mm/min. The minimum relative area for the compression stage was controlled at 52.5%. During the interface compression-expansion cycles, IRRAS measurements of the monolayer were continuously performed with an acquisition time of ~57 s/spectrum. Within each IRRAS spectrum acquisition period, there is no indication of significant signal interference caused by the monolayer composition or surface concentration variation under the interface compression or expansion condition. The compression or expansion rate is much slower than that under physiological conditions. However, a higher rate may result in unavoidable signal interference due to interface perturbation and monolayer composition or surface concentration variation during the spectrum acquisition.

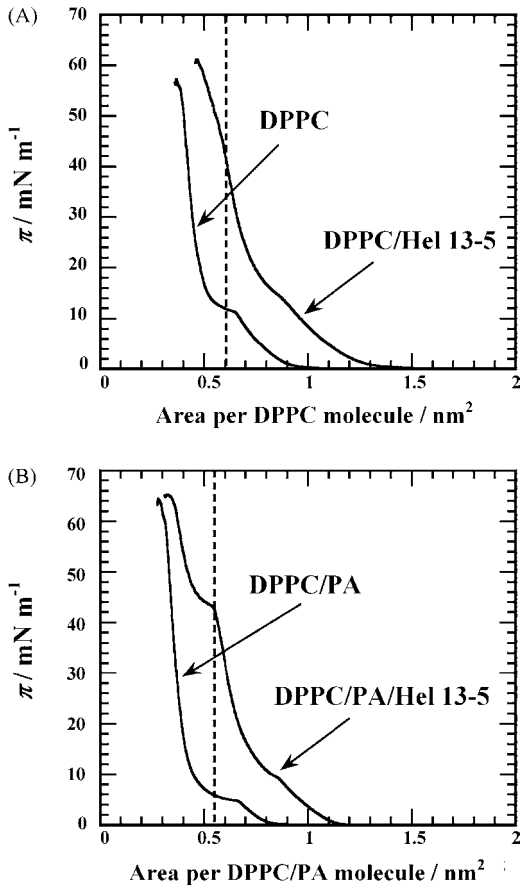


**Fig. 1.** Surface pressure ($\pi$)–area ($A$) isotherms of the binary DPPC/Hel 13-5 (A) and the ternary DPPC/PA/Hel 13-5 systems (B) on a 0.02 M Tris buffer solution (pH 7.4) with 0.13 M NaCl at 298.2 K; (A) pure DPPC and $X_{\text{Hel 13-5}} = 0.1$, and (B) DPPC + 10 wt.% PA mixture and $X_{\text{Hel 13-5}} = 0.1$. Abscissas denote the area per DPPC molecule (A) and per DPPC/PA molecule, respectively. The dashed lines indicate the onset area of the squeeze-out phenomenon at ~0.60 (A) and ~0.55 nm$^2$ (B).

## 3. Results and discussion

### 3.1. Surface pressure–area isotherms

Fig. 1 shows surface pressure ($\pi$)–area ($A$) isotherms of pure DPPC, DPPC/Hel 13-5 ($X_{\text{Hel 13-5}} = 0.1$), DPPC/PA (or DPPC + 10 wt.% PA), and DPPC/PA/Hel 13-5 ($X_{\text{Hel 13-5}} = 0.1$) mixtures. The previous data were partially utilized and reconstructed in Figure 1 [24,32,33]. Note that area axes are recalculated to area per DPPC molecule (Fig. 1A) or per DPPC/PA molecule (Fig. 1B). This is because of quantitative analyses on the effect of Hel 13-5 addition to the lipid molecules by IRRAS techniques. The $\pi$–$A$ isotherm of DPPC monolayers indicated a liquid expanded (LE)/liquid condensed (LC) transition at ~12 mN m$^{-1}$ (Fig. 1A). On further compression, the surface pressure reached ~55 mN m$^{-1}$ within the monolayer state. When a small amount of Hel 13-5 ($X_{\text{Hel 13-5}} = 0.1$) was added to DPPC, the $\pi$–$A$ isotherm shifted to larger areas and the transition pressure increased to ~14 mN m$^{-1}$. It is noted that the isotherm of $X_{\text{Hel 13-5}} = 0.1$ has a plateau region at ~42 mN m$^{-1}$, where Hel 13-5 starts to be squeezed-out of surface monolayers into subphase [24,33]. This phenomenon is very important for pulmonary functions to prevent lung collapse under exhalation. The compression beyond the point that area was indicated by a dashed line facilitated the squeeze-out motion to increase the surface concentration of DPPC. That is, the surface is refined to DPPC monolayers and the excluded Hel 13-5 forms a surface-related reservoir at the adjacent monolayer to stabilize the film [24,38–40]. Then, in the case of film expansion, close-packed monolayers could rapidly respread to the surface with a short delay. Thus, the $\pi$–$A$ isotherm for pulmonary surfactant systems indicates hysteresis behavior during repeated compression and expansion [24,34–36]. This elegant action is associated with the retention of physical homeostasis of lungs.

The PA addition to pulmonary surfactant preparations is commonly thought to improve the packing state of saturated phospholipid monolayers. Therefore, in the present study, the lipid mixtures of DPPC + 10 wt.% PA with or without Hel 13-5 ($X_{\text{Hel 13-5}} = 0$ or 0.1) were also employed to elucidate the orientation of the DPPC/PA aliphatic chains. As shown in Fig. 1B, the DPPC/PA monolayer had the LE/LC transition pressure of ~5 mN m$^{-1}$ and the collapse pressure of ~60 mN m$^{-1}$. The small addition of Hel 13-5 ($X_{\text{Hel 13-5}} = 0.1$) shifted the $\pi$–$A$ isotherm to larger areas and increased the transition pressure to ~9 mN m$^{-1}$. Similarly to the DPPC/Hel 13-5 system, the DPPC/PA/Hel 13-5 preparation had the clearer onset of the Hel 13-5 squeeze-out action at ~42 mN m$^{-1}$. Beyond the surface pressure, the surface is refined to DPPC/PA monolayers. Considering subphase pH in the current condition, during the squeeze-out motion, parts of dissociated PA molecules are excluded together with Hel 13-5 from the surface monolayers. This was supported by the evidence that the area difference between both $\pi$–$A$ isotherms in Fig. 1B at higher surface pressures (>50 mN m$^{-1}$) was smaller compared with the DPPC/Hel 13-5 systems (Fig. 1A). In the previous paper [32], it had been concluded that all of PA molecules located at the interface above ~42 mN m$^{-1}$. Judging from the present quantitative analyses with *in situ* IRRAS, however, it is a new finding that parts of dissociated PA molecules are excluded below the interface, where the remaining PA components exist in the surface monolayers.

### 3.2. Hysteresis behavior of DPPC/Hel 13-5 monolayers

The reflectance–absorbance (RA) intensity is equal to -log ($R/R_0$), where $R$ and $R_0$ are the reflectivities of the monolayer-covered and pure buffer solution surfaces, respectively. The original IRRAS data were plotted as RA intensity versus wavenumber as shown in Fig. 2, where the spectra of spread DPPC monolayers prior to film compression and at the compressed state were presented. Both the spectra had specific peaks of an asymmetric methylene stretching vibration ($\nu_a$-$CH_2$) at ~2920 cm$^{-1}$ and of a symmetric methylene

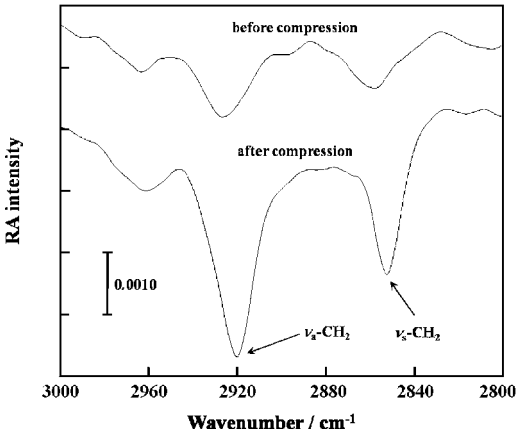


**Fig. 2.** IRRAS spectra of the methylene stretching band region (2800–3000 cm$^{-1}$) for pure DPPC monolayers spread on a $NaH_2PO_4/Na_2HPO_4$ buffer solution (pH 7.0) at room temperature (~303.2 K). The representative spectra before ($A$ = ~0.86 nm$^2$) and after compression ($A$ = ~0.45 nm$^2$) are presented. The antisymmetric methylene stretching vibration ($\nu_a$-$CH_2$) at ~2920 cm$^{-1}$ is indicated by an arrow. The bar reflects the intensity in reflectance–absorbance unit.

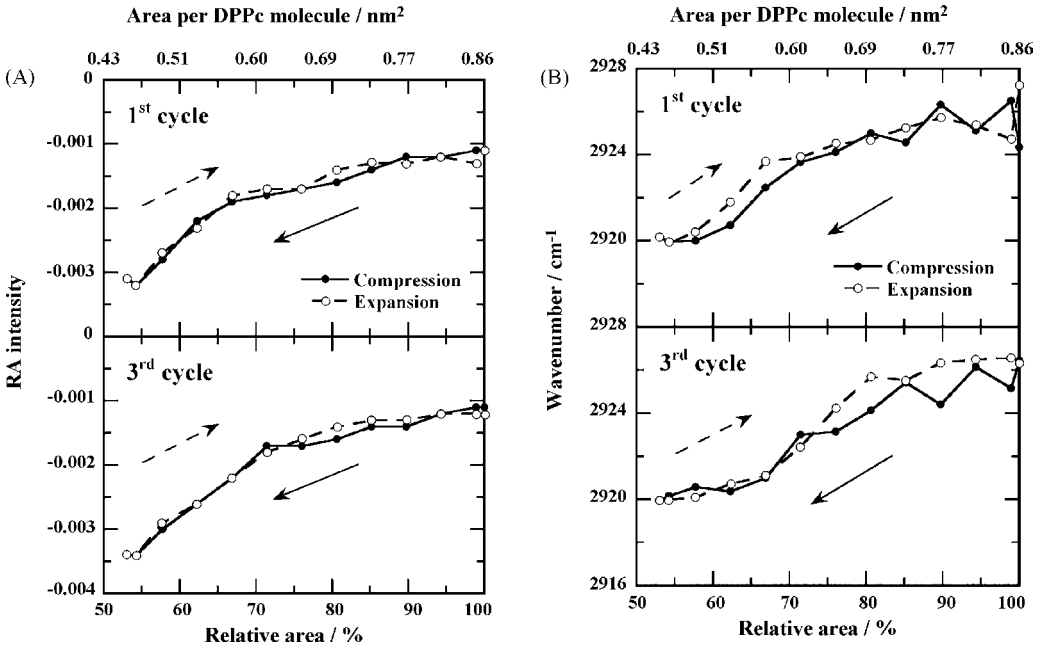


**Fig. 3.** Consecutive $\nu_a$-$CH_2$ RA intensity–relative area (A) and $\nu_a$-$CH_2$ wavenumber–relative area curves (B) of a DPPC monolayer with an initial area per molecule of 0.86 nm$^2$. The relative area represents the ratio of the actual interfacial area during the compression-expansion cycle. Upper abscissa is labeled by the calculated area per DPPC molecule.

stretching vibration ($\nu_s$-$CH_2$) at ~2850 cm$^{-1}$. The $\nu_a$-$CH_2$ peak with larger absolute values and better sensitivities is easy to probe the change in surface DPPC concentrations upon compression compared with the $\nu_s$-$CH_2$ peak, although both the peaks can reflect it [29]. Thus, the $\nu_a$-$CH_2$ RA intensity and its wavenumber were utilized to perform the IRRAS analysis for the present systems.

The repeated compression-expansion behavior of pure DPPC monolayers at the air–water interface is shown as a plot of the $\nu_a$-$CH_2$ RA intensity against relative trough area (Fig. 3). The representative data of the first and the third cycles are presented and upper abscissa is labeled by the calculated area per DPPC molecule in the figure. All of the $\nu_a$-$CH_2$ RA intensity data obtained in the present study included an uncertainty of 0.0002 [27,28]. The absorption bands of monolayers at the interface are negative, and the basis for the negative absorbance in the monolayer spectra has been explored [27,28]. As shown in Fig. 3A, the initial absolute RA value of the $\nu_a$-$CH_2$ band for a DPPC monolayer at ~0.86 nm$^2$/molecule was 0.0011. Upon compression, the absolute RA value increased gradually and reached 0.0032 at ~0.45 nm$^2$/molecule (before the collapse area). This is expected

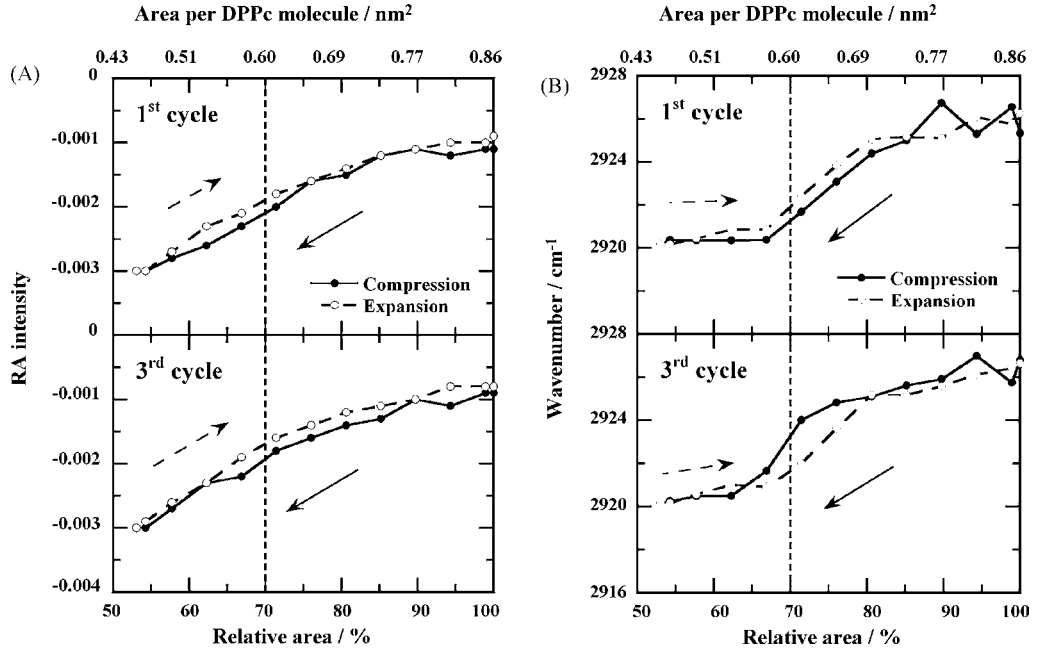


**Fig. 4.** Consecutive $\nu_a$-$CH_2$ RA intensity–relative area (A) and $\nu_a$-$CH_2$ wavenumber–relative area curves (B) of a binary DPPC/Hel 13-5 monolayer at $X_{Hel\ 13\text{-}5}$ = 0.1 with an initial area per DPPC molecule of 0.86 nm$^2$. The onset area of the squeeze-out phenomenon is indicated by dashed lines (0.60 nm$^2$). Upper abscissa is labeled by the calculated area per DPPC molecule.

because a higher surface concentration of molecules always results in a stronger RA response. During the expansion stages, the absolute RA intensity coincided with that under film compression due to the insufficient compression of the monolayer. The monolayer compression beyond the DPPC collapse pressure induced a loss of free DPPC molecules during the cycle [29]. Thus, the analogy of the $\nu_a$-$CH_2$ value between the first cycle and the third cycle indicates no loss of the DPPC molecules. As for Figs. 3 and 4, note that a spread amount of DPPC was kept constant in both pure DPPC and the DPPC/Hel 13-5 mixture ($X_{Hel\ 13\text{-}5} = 0.1$) to perform the quantitative comparison between their IR intensities.

The corresponding $\nu_a$-$CH_2$ wavenumber versus relative area for DPPC monolayers is plotted in Fig. 3B. At the beginning of the first compression, the maximum in wavenumber was ~2926 $cm^{-1}$. The wavenumber decreased with shifting to small area upon compression, and a value of 2920 $cm^{-1}$ was found at the end of the first compression stage. It has been reported that the wavenumber corresponding to the minimum in the $\nu_a$-$CH_2$ band is sensitive to the packing, the orientation, and the conformational change of the molecular acyl chains in the monolayer state, and a lower wavenumber is a characteristic of the highly ordered conformation (or the all-*trans* conformation) of the aliphatic chains [41–44]. Therefore, the decreasing behavior demonstrated that the DPPC molecules became oriented well on compression. In the first expansion, the wavenumber increased with an increase in relative area to accord with those in the corresponding compression. The same behavior was also observed in the third cycle, suggesting that the variation in the orientation of DPPC acyl chains during repeated compression and expansion process occurred reversibly.

For the binary DPPC/Hel 13-5 monolayer at $X_{Hel\ 13\text{-}5} = 0.1$, the hysteresis curves of $\nu_a$-$CH_2$ RA intensity with relative area are plotted in Fig. 4A. As seen in Fig. 1A, the figure also contained dashed lines at ~0.60 $nm^2$/molecule, where Hel 13-5 states to be squeezed-out of surface monolayers [24,33]. Similarly to pure DPPC, the initial absolute RA value of the binary monolayer was 0.0011 due to the same surface amount as the pure DPPC system. Upon compression, the absolute RA value increased gradually and reached 0.0030 at ~0.45 $nm^2$/molecule, where the monolayers were in the closed-packed state. This value was the same as that in the DPPC system at ~0.45 $nm^2$/molecule. That is, no loss of DPPC upon compression was observed at the air/liquid interface. This result supported that the surface was refined to DPPC monolayers and almost all Hel 13-5 were squeezed-out into subphase. These plots in the first and the third cycles showed the same behavior. It indicates that Hel 13-5 makes DPPC molecules in the solid monolayer state respread to the interface, repeatedly.

For hysteresis curves of the corresponding $\nu_a$-$CH_2$ wavenumber with relative area (Fig. 4B), on the other hand, the interesting behavior was observed in the squeeze-out regions. Upon the first compression, the wavenumber decreased gradually as the same in pure DPPC system. Beyond the onset of the squeeze out indicated by dashed lines, however, the wavenumber kept the value of ~2920 $cm^{-1}$ regardless of shifting to small areas. This demonstrated that the orientation for hydrophobic chains of DPPC became in the most packed state soon after emergence of the Hel 13-5 squeeze-out action and the packed orientation continued up to the collapse state of the binary monolayer at ~0.45 $nm^2$/molecule. During this surface refinement, Hel 13-5 was gradually excluded to subphase with orientation and conformation for DPPC aliphatic chains sustained. For the third cycle, the similar behavior was observed. It supports the fact that the reversible change in the orientation and the good respreading ability of the binary monolayer exist [24,33].

### 3.3. Hysteresis behavior of DPPC/PA/Hel 13-5 monolayers

Shown in Figure 5A are the $\nu_a$-$CH_2$ RA intensities versus relative area for the lipid mixture of DPPC + 10 wt.% PA at first and third cycles. To carry out the quantitative comparison between the DPPC/PA mixtures with and without Hel 13-5, a spread amount of DPPC/PA was fixed in between Figs. 5 and 6. Thus, upper abscissa is labeled by the calculated area per DPPC/PA molecule. For the DPPC/PA monolayer, the initial absolute RA value of the $\nu_a$-$CH_2$ band at ~0.65 $nm^2$/molecule was 0.0017. Upon compression, the absolute RA value increased gradually and then reached 0.0050 at ~0.35 $nm^2$/molecule, where the monolayer was in the close-packed

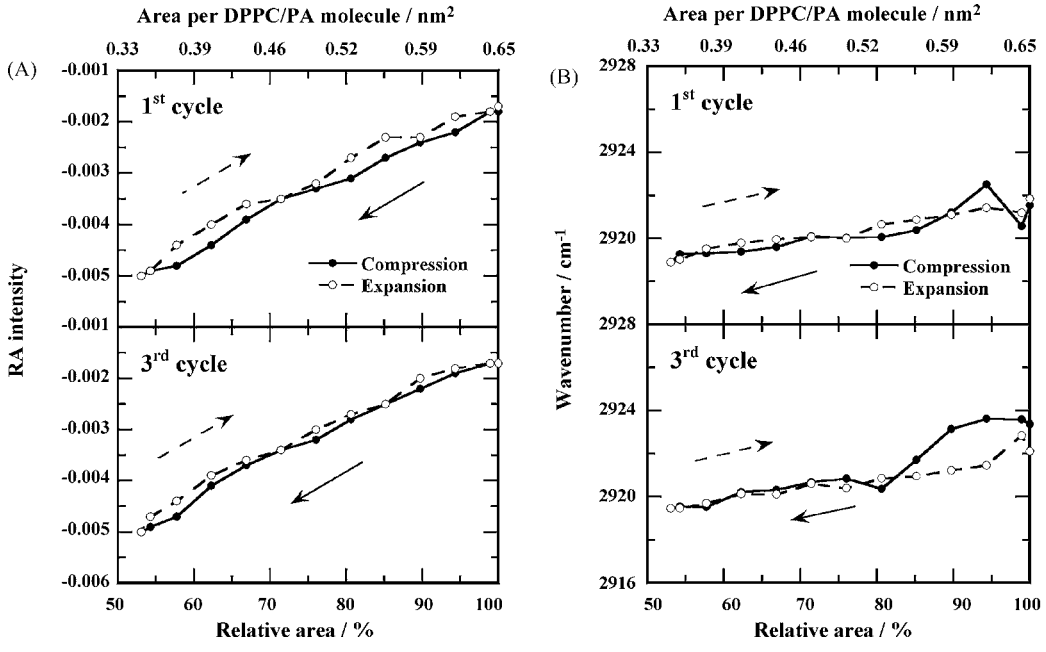


**Fig. 5.** Consecutive $\nu_a$-$CH_2$ RA intensity–relative area (A) and $\nu_a$-$CH_2$ wavenumber–relative area curves (B) of DPPC + 10 wt.% PA with an initial area per molecule of 0.65 $nm^2$. Upper abscissa is labeled by the calculated area per DPPC/PA molecule.

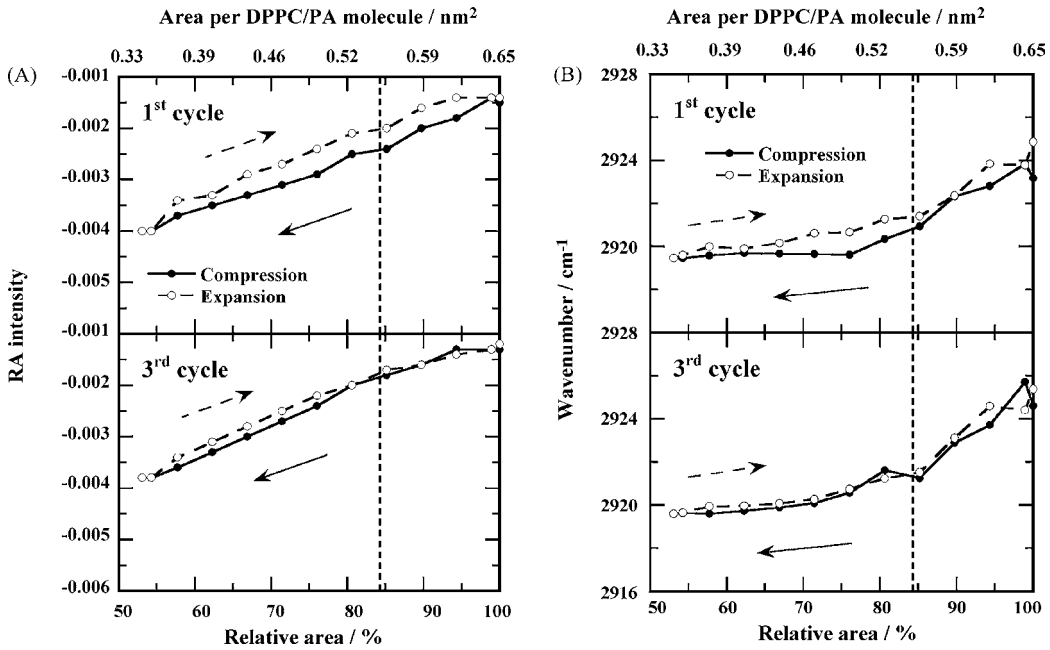


**Fig. 6.** Consecutive $\nu_a$-$CH_2$ RA intensity–relative area (A) and $\nu_a$-$CH_2$ wavenumber–relative area curves (B) of a ternary DPPC/PA/Hel 13-5 monolayer at $X_{Hel\ 13\text{-}5} = 0.1$ with an initial area per DPPC/PA molecule of 0.65 $nm^2$. The onset area of the squeeze-out phenomenon is indicated by dashed lines (0.55 $nm^2$). Upper abscissa is labeled by the calculated area per DPPC/PA molecule.

state (see Fig. 1). When the films were expanded, the absolute RA intensity decreased to reach the initial value. In addition, this behavior was reproducible from the first to the third cycles. Thus, it is also suggested that no quantitative loss of DPPC and PA molecules from the surface during compression-expansion cycles occurs in the monolayer.

Fig. 5B presents the plots of the corresponding $\nu_a$-$CH_2$ wavenumber with relative area for the DPPC/PA monolayer. Under the first compression, the $\nu_a$-$CH_2$ wavenumber slightly decreased from 2922 to 2919 $cm^{-1}$. The slight reduction is resulted from the lower compressibility of the DPPC/PA monolayer compared with the DPPC monolayer. During the first expansion, the wavenumber increased with an increase in relative area to accord with those under the corresponding compression. The good reproducibility between the first and the third cycles indicates the reversible orientational variation in acyl chains for DPPC and PA during repeated cycles.

The hysteresis curves of $\nu_a$-$CH_2$ RA intensity with relative area for the ternary DPPC/PA/Hel 13-5 monolayer at $X_{Hel\ 13\text{-}5} = 0.1$ are shown in Fig. 6A. As seen in Fig. 1B, the dashed lines mean the molecular area of ~0.55 $nm^2$/molecule, where the squeeze-out action of Hel 13-5 states to occur. The absolute RA values increased from 0.0015 to 0.0040 with decreasing relative area. It is quite interesting that at the close-packed state of monolayers, the value of 0.0040 was smaller compared with that for the DPPC/PA mixture (difference: 0.0010). Furthermore, the trend was reproducible from the first to the third cycles. If only the peptides are squeezed-out of surface monolayers, the absolute RA value should reach ~0.0050 due to the surface refinement to binary DPPC/PA mixtures. Consequently, it is suggested that Hel 13-5 is excluded together with parts of dissociated PA molecules from the surface to form the surface-associated aggregates. This action is also reversible and the dissociated PA molecules utilized into the aggregates can steadily respread to the surface.

The corresponding $\nu_a$-$CH_2$ wavenumber versus relative area for the DPPC/PA/Hel 13-5 mixture ($X_{Hel\ 13\text{-}5} = 0.1$) is plotted in Fig. 6B. In analogy with the DPPC/PA mixture, the wavenumber of DPPC/PA/Hel 13-5 slightly decreased from 2923 to 2919 $cm^{-1}$ on the first compression. However, the reduction mode is different in the vicinity of the squeeze-out area indicated by dashed lines. That is, in the squeeze-out region, the wavenumber showed almost the same value of ~2920 $cm^{-1}$ despite the film compression. This means that the aliphatic chain orientation of DPPC/PA is kept in the close-packed state. Under the situation, the squeeze-out motion of Hel 13-5 together with dissociated PA molecules occurs and the surface is gradually refined to the monolayer of DPPC and undissociated PA molecules. These motions across the surface are reversible without loss of materials. The events are also observed in the binary DPPC/Hel 13-5 system. Therefore, it is demonstrated that close-packed orientation of acyl chains at the surface triggers an ejected movement of the proteins or peptides (with positive charges) together with negatively charged molecules or LE components.

## 4. Conclusions

The hysteresis behavior for the binary DPPC/Hel 13-5 and the ternary DPPC/PA/Hel 13-5 monolayers at the air–water interface was probed directly by an IRRAS technique. These data were compared with those of the equivalent DPPC and DPPC/PA mixtures, respectively. For the $\nu_a$-$CH_2$ RA intensity of both mixtures at $X_{Hel\ 13\text{-}5} = 0.1$, the absolute RA values increased with shifting to small area, monotonously. For the corresponding wavenumber, on the other hand, the values decreased gradually at the same as pure DPPC and DPPC/PA systems upon compression up to the onset of the squeeze-out phenomenon. However, they were kept constant in the squeeze-out region. These results suggested that the acyl chain orientation of DPPC and DPPC/PA became in the close-packed state soon after occurrence of the squeeze-out behavior and the packed orientation was retained up to the collapse state of monolayers. This indicates that the squeezed-out molecules stabilize the monolayers left at the interface. Furthermore, the similar behavior from the first to the third cycles supports the good respreading ability of the preparations treated in this study. Judging from the data for

the DPPC/PA/Hel 13-5 systems, it is demonstrated that undissociated PA molecules are useful for accomplishment of close-packed orientation of DPPC aliphatic chains at the surface, whereas dissociated PA components contribute to the squeeze-out motion of Hel 13-5 to form 3-D aggregates associated with surface monolayers.

## Acknowledgements

This work was supported by a Grant-in-Aid for Scientific Research 20500414 from the Japan Society for the Promotion of Science (JSPS). This work was also supported by a Grant-in-Aid for Young Scientists 20810041 from JSPS (H.N.).

## References

[1] R. Veldhuizen, K. Nag, S. Orgeig, F. Possmayer, Biochim. Biophys. Acta 1408 (1998) 90–108.
[2] P. Krüger, J.E. Baatz, R.A. Dluhy, M. Lösche, Biophys. Chem. 99 (2002) 209–228.
[3] S.-H. Yu, F. Possmayer, J. Lipid Res. 44 (2003) 621–629.
[4] B. Fleming, K.M.W. Keough, Chem. Phys. Lipids 49 (1988) 81–86.
[5] R. Chang, S. Nir, F.R. Poulain, Biochim. Biophys. Acta 1371 (1998) 254–264.
[6] M.A. Oosterlaken-Dijksterhuis, H.P. Haagsman, L.M.G. Van Golde, R.A. Demel, Biochemistry 30 (1991) 8276–8281.
[7] J. Ma, S. Koppenol, H. Yu, G. Zografi, Biophys. J. 74 (1998) 1899–1907.
[8] D.O. Grigoriev, J. Kragel, A.V. Akentiev, B.A. Noskov, R. Miller, U. Pison, Biophys. Chem. 104 (2003) 633–642.
[9] H. Nakahara, S. Lee, G. Sugihara, C.-H. Chang, O. Shibata, Langmuir 24 (2008) 3370–3379.
[10] G. Brezesinski, A. Dietrich, B. Struth, C. Boehm, W.G. Bouwman, K. Kjaer, H. Moehwald, Chem. Phys. Lipids 76 (1995) 145–157.
[11] U. Dahmen-Levison, G. Brezesinski, H. Möhwald, Colloids Surf. A 171 (2000) 97–103.
[12] J. Zhao, D. Vollhardt, G. Brezesinski, S. Siegel, J. Wu, J.B. Li, R. Miller, Colloids Surf. A 171 (2000) 175–184.
[13] K.Y.C. Lee, A. Gopal, A. von Nahmen, J.A. Zasadzinski, J. Majewski, G.S. Smith, P.B. Howes, K. Kjaer, J. Chem. Phys. 116 (2002) 774–783.
[14] S. Taneva, K.M. Keough, Biophys. J. 66 (1994) 1137–1148.
[15] F. Bringezu, J. Ding, G. Brezesinski, J.A. Zasadzinski, Langmuir 17 (2001) 4641–4648.
[16] G. Gorree, J. Egberts, G. Bakker, A. Beintema, M. Top, Biochim. Biophys. Acta 1086 (1991) 209–216.
[17] A.M. Cockshutt, D.R. Absolom, F. Possmayer, Biochim. Biophys. Acta 1085 (1991) 248–256.
[18] S. Nakamura, H. Nakahara, M.P. Krafft, O. Shibata, Langmuir 23 (2007) 12634–12644.
[19] D. Hönig, D. Möbius, J. Phys. Chem. 95 (1991) 4590–4592.
[20] S. Hénon, J. Meunier, Rev. Sci. Instrum. 62 (1991) 936–939.
[21] H.M. McConnell, Annu. Rev. Phys. Chem. 42 (1991) 171–195.
[22] Y. Matsumoto, H. Nakahara, Y. Moroi, O. Shibata, Langmuir 23 (2007) 9629–9640.
[23] T. Hiranita, S. Nakamura, M. Kawachi, H.M. Courrier, T.F. Vandamme, M.P. Krafft, O. Shibata, J. Colloid Interface Sci. 265 (2003) 83–92.
[24] H. Nakahara, S. Nakamura, T. Hiranita, H. Kawasaki, S. Lee, G. Sugihara, O. Shibata, Langmuir 22 (2006) 1182–1192.
[25] H. Nakahara, S. Nakamura, H. Kawasaki, O. Shibata, Colloids Surf. B 41 (2005) 285–298.
[26] J.Y. Josefowicz, N.C. Maliszewskyj, S.H.J. Idziak, P.A. Heiney, J.P. McCauley Jr., A.B. Smith III, Science 260 (1993) 323–326.
[27] R.A. Dluhy, D.G. Cornell, J. Phys. Chem. 89 (1985) 3195–3197.
[28] R.A. Dluhy, J. Phys. Chem. 90 (1986) 1373–1379.
[29] C.-L. Yin, C.-H. Chang, Langmuir 22 (2006) 6629–6634.
[30] C. Wang, J. Zheng, L. Zhao, V.K. Rastogi, S.S. Shah, J.J. Defrank, R.M. Leblanc, J. Phys. Chem. B 112 (2008) 5250–5256.
[31] C. Wang, M. Micic, M. Ensor, S. Daunert, R.M. Leblanc, J. Phys. Chem. B 112 (2008) 4146–4151.
[32] H. Nakahara, S. Lee, G. Sugihara, O. Shibata, Langmuir 22 (2006) 5792–5803.
[33] H. Nakahara, S. Nakamura, S. Lee, G. Sugihara, O. Shibata, Colloids Surf. A 270–271 (2005) 52–60.
[34] R. Wüstneck, N. Wüstneck, B. Moser, U. Pison, Langmuir 18 (2002) 1125–1130.
[35] R. Wüstneck, N. Wüstneck, B. Moser, V. Karageorgieva, U. Pison, Langmuir 18 (2002) 1119–1124.
[36] N. Wüstneck, R. Wüstneck, V.B. Fainerman, R. Miller, U. Pison, Colloids Surf. B 21 (2001) 191–205.
[37] T. Kiyota, S. Lee, G. Sugihara, Biochemistry 35 (1996) 13196–13204.
[38] C. Alonso, T. Alig, J. Yoon, F. Bringezu, H. Warriner, J.A. Zasadzinski, Biophys. J. 87 (2004) 4188–4202.
[39] J. Ding, I. Doudevski, H.E. Warriner, T. Alig, J.A. Zasadzinski, A.J. Waring, M.A. Sherman, Langmuir 19 (2003) 1539–1550.
[40] R.V. Diemel, M.M.E. Snel, A.J. Waring, F.J. Walther, L.M.G. van Golde, G. Putz, H.P. Haagsman, J.J. Batenburg, J. Biol. Chem. 277 (2002) 21179–21188.
[41] X. Wen, J. Lauterbach, E.I. Franses, Langmuir 16 (2000) 6987–6994.
[42] M.L. Mitchell, R.A. Dluhy, J. Am. Chem. Soc. 110 (1988) 712–718.
[43] R. Mendelsohn, J.W. Brauner, A. Gericke, Annu. Rev. Phys. Chem. 46 (1995) 305–334.
[44] A. Gericke, H. Hühnerfuss, J. Phys. Chem. 97 (1993) 12899–12908.